INVITED PAPER *Special Section on Analog Circuits and Their Application Technologies*

Transmission Line Coupler: High-Speed Interface for Non-Contact Connecter

Mototsugu HAMADA[†a)], ***Nonmember and*** **Tadahiro KURODA**[†], ***Fellow***

SUMMARY This paper describes transmission line couplers for non-contact connecters. Their characteristics are formulated in closed forms and design methodologies are presented. As their applications, three different types of transmission line couplers, two-fold transmission line coupler, single-ended to differential conversion transmission line coupler, and rotatable transmission line coupler are reviewed.

key words: *transmission line coupler, non-contact connecter, interface, transceiver*

1. Introduction

The interconnection has been always the bottleneck of system performance. The idea of integrated circuits comes from the difficulties of the interconnection of vacuum tubes. Though the device performance of a silicon transistor was worse than that of a vacuum tube, silicon integrated circuits replaced most of the applications of vacuum tubes. The scaling of CMOS technology has increased the number of transistors integrated on a chip with a rate of 50%/year and the operation frequency with a rate of 14%/year. However we now stand on the cliff of Moore's Law and Dennard's Scaling Law. When it is very difficult to increase the system integration level on a chip, we need to implement a system with combining two or more sub-systems. At this point, the interconnection between sub-systems is again the bottleneck of the total system performance. Our group proposed two solutions for this, TCI (ThruChip Interface) for inter-chip communications [1] and TLC (Transmission Line Coupler) for inter-board communications [2]. In this paper, we will review TLC.

As CMOS technology scales, the bit rate of communication between boards has reached around 20Gbps. For example, PCI express 4.0 is 16GTps per direction [3]. Meanwhile such a high-speed signal is susceptible to the condition of the signal line, and issues such as decay, distortion, and reflections arise. With the increase of the data rate, the design of signal lines and connectors becomes more difficult, which brings the increase of the cost by employing expensive low-loss substrate materials and the increase of the footprint due to a special layout for impedance matching. However, it is still difficult to control the impedance at a conventional connector due to its mechanical structure. In addition, it has a contact of exposed metals, which is susceptible to moisture causing metal corrosion, and subject to wear, corruption, and electrostatic destruction due to human body discharge.

TLC is a solution of the problem described above. TLC utilizes a near-field electromagnetic effect between couplers. The radiated power is very weak so that a far-field electromagnetic effect is negligible. We can arrange multiple couplers in parallel without suffering from crosstalk. The coupler is implemented with traces on PCB only with an additional cost of its footprint. It does not require any other housings or mechanical structures, nor soldering, which minimizes the additional assembly cost. It does not suffer from wear, corruption and is waterproof since there is no exposed electrodes. Besides, it can connect devices having different DC levels since it is an AC-coupled connection. Contactless baseband communication techniques utilizing coils or capacitors have a restriction of the maximum bit rate limited by their self-resonant frequency and their frequency dependence of the characteristic impedance. On the other hand, TLC is a wideband impedance-matched coupler, solving the problem that an L/C-coupled techniques face. Since the coupler consists of transmission lines, the characteristic impedance is almost constant against frequency. Therefore the impedance matching is achieved over a wide frequency range, mitigating signal reflections. The transmission line itself does not exhibits self-resonance by parasitic capacitance and inductance. By utilizing the wideband characteristic of TLC, a high-speed/lowpower contactless baseband communication can be achieved.

This paper is organized as follows: Section 2 discusses the basics of TLC where characteristics are formulated in closed forms and its design methodology is presented. In Sect. 3, we review three different types of applications, two-fold transmission line coupler, single-ended to differential conversion transmission line coupler, and rotatable transmission line coupler. Section 4 concludes this paper.

2. Basics of Transmission Line Coupler

2.1 Overview

We proposed a transmission line coupler (TLC) for a contactless high-speed interface that utilizes crosstalk between transmission lines [3]. Figure 1 shows the structure of a TLC and its equivalent circuit. The signal is transferred in a differential mode through distributed capacitance and

Manuscript received December 17, 2018.
Manuscript revised February 12, 2019.
[†]The authors are with Keio University, Yokohama-shi, 223–8522 Japan.
a) E-mail: hamada@kuroda.elec.keio.ac.jp
DOI: 10.1587/transele.2018CTI0002

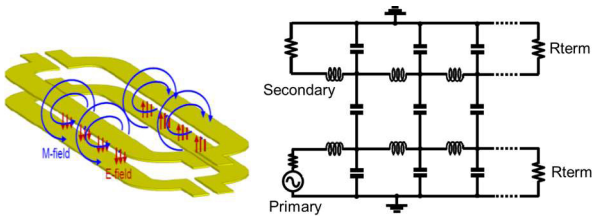

Fig. 1 Structure and equivalent circuit of TLC.

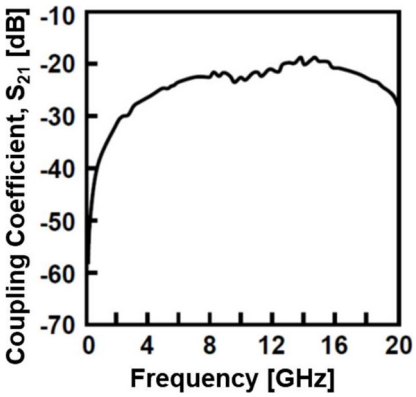

Fig. 2 Frequency response of TLC.

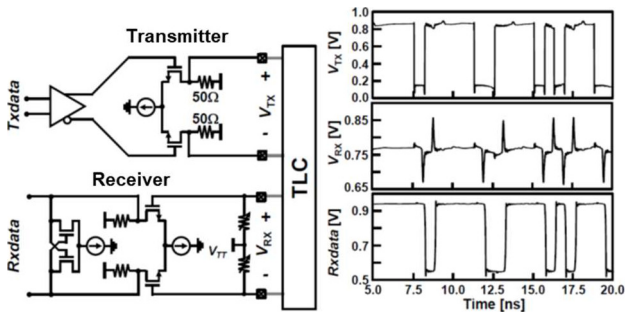

Fig. 3 Circuit diagram of TLC transceiver and simulation results.

inductance. They also define the characteristic impedance of the transmission line. With an appropriate design, the TLC can be impedance-matched to the signal source. Figure 2 shows S_{21} of a TLC, which exhibits wideband characteristics and mitigates reflections. The TLC is horse shoe-shaped transmission lines. The width of transmission lines is wider in the coupler so that the coupling coefficient can be larger. While the coupling coefficient depends on the width of transmission lines of the coupler, the bandwidth depends on its length. Therefore the communication distance, i.e. the gap in the coupler, can be increased without sacrificing the bandwidth. Figure 3 shows circuit diagrams of a transmitter and a receiver, and simulation results. In this simulation, non-return-to-zero (NRZ) signal is applied to the TLC via a 50-Ω output transmitter. Since the TLC has a highpass transfer function, the received waveform, V_{RX}, is a first order differentiation of the transmitted waveform. The receiver consists of a hysteretic comparator and an amplifier. The

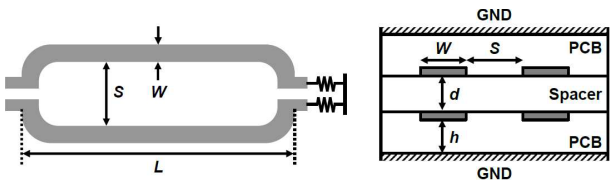

(a) top view (b) side view

Fig. 4 Structure and design parameters of TLC.

hysteresis, V_{HYS}, discriminate between signals and noises such as inter-symbol interferences and reflections. When the amplitude of the received signal, V_{RX} is larger than V_{HYS}, the comparator flips its output. Thus, the transmitted data is recovered at the receiver side by detecting the differentiated signal. As a baseband communication requires no modulation/demodulation circuits, the number of transistor required in the circuit is small as shown in Fig. 3, therefore the power consumption of the transceiver is also small.

2.2 Formulation

A basic TLC structure is shown in Fig. 4. A TLC is a horse shoe-shaped pair of microstrip lines. A wide line width helps increase the coupling coefficient between the primary and the secondary. Besides, the horse shoe shape helps decrease the coupling between differential lines. It shows a top view and a side view of a TLC. The performance of a TLC depends on width of differential lines, W, spacing between the lines, S, length of the lines, L, distance between the primary and the secondary, d, height from the ground plane of a PCB, h, and relative permittivity ε_{r_space}. More precisely, the coupling coefficient depends on line width W, spacing S, distance d, and ground height h, while the frequency response, i.e. the center frequency (f_c), and the bandwidth depends on length L. Since the frequency response and the coupling coefficient can be independently designed, the communication distance d can be increased without sacrificing the data rate.

As shown in Fig. 4, the primary and the secondary are coupled both electrically and magnetically. When a signal is applied to the primary, voltage change is transferred as current change via a coupling capacitor and current change is transferred as voltage change via magnetic coupling to the secondary. The received signal on the secondary is the addition of both effects. From the equivalent circuit shown in Fig. 5, the following equation is derived [4].

$$\begin{aligned}\frac{\partial}{\partial z}\begin{bmatrix}V_1\\V_2\end{bmatrix} &= -\frac{\partial}{\partial t}\begin{bmatrix}L_{11} & L_{21}\\L_{21} & L_{22}\end{bmatrix}\begin{bmatrix}I_1\\I_2\end{bmatrix}\\ \frac{\partial}{\partial z}\begin{bmatrix}I_1\\I_2\end{bmatrix} &= -\frac{\partial}{\partial t}\begin{bmatrix}C_{11} & C_{21}\\C_{21} & C_{22}\end{bmatrix}\begin{bmatrix}V_1\\V_2\end{bmatrix}.\end{aligned} \tag{1}$$

Current change and voltage change are a linear combination of an ascending wave, a_i, and a descending wave, b_i, in Fig. 5. They are expressed by the characteristic impedance, Z_i, as follows.

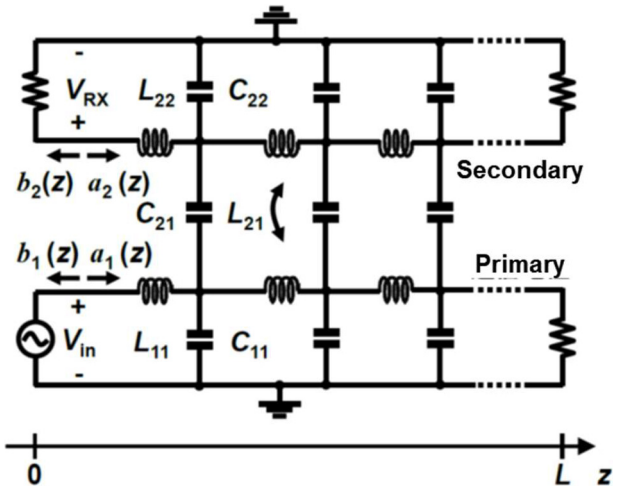

Fig. 5 Equivalent circuit of TLC.

$$a_i(Z) = \frac{V_i + Z_i I_i}{\sqrt{2Z_i}},\ b_i(Z) = \frac{V_i - Z_i I_i}{\sqrt{2Z_i}}. \tag{2}$$

With Eqs. (1) and (2), the ascending and descending waves are expressed as follows.

$$\begin{aligned}\frac{\partial}{\partial z}\begin{bmatrix} a_1 \\ a_2 \end{bmatrix} &= -\mathrm{j}\begin{bmatrix} \beta_1 & C \\ C & \beta_2 \end{bmatrix}\begin{bmatrix} a_1 \\ a_2 \end{bmatrix} + \mathrm{j}\begin{bmatrix} 0 & L \\ L & 0 \end{bmatrix}\begin{bmatrix} b_1 \\ b_2 \end{bmatrix} \\ \frac{\partial}{\partial z}\begin{bmatrix} b_1 \\ b_2 \end{bmatrix} &= -\mathrm{j}\begin{bmatrix} 0 & L \\ L & 0 \end{bmatrix}\begin{bmatrix} a_1 \\ a_2 \end{bmatrix} + \mathrm{j}\begin{bmatrix} \beta_1 & C \\ C & \beta_2 \end{bmatrix}\begin{bmatrix} b_1 \\ b_2 \end{bmatrix}\end{aligned} \tag{3}$$

where

$$C = \frac{1}{2}\sqrt{\beta_1\beta_2}\,(K_L - K_C),\ L = \frac{1}{2}\sqrt{\beta_1\beta_2}\,(K_L + K_C). \tag{4}$$

Magnetic coupling coefficient, K_L, capacitive coupling coefficient, K_C and phase constant of ascending and descending waves, β_i, are expressed as follows.

$$\begin{aligned} K_L &= \frac{L_{21}}{\sqrt{(L_{11}+L_{21})(L_{22}+L_{21})}}, \\ K_C &= \frac{C_{21}}{\sqrt{(C_{11}+C_{21})(C_{22}+C_{21})}} \\ \beta_i &= \omega\sqrt{(L_{ii}+L_{21})(C_{ii}+L_{21})}. \end{aligned} \tag{5}$$

Supposing that relative permittivity of the material between the primary and the secondary and the material of PCB are same, K_L equals to K_C, ($K = K_L = K_C$) [4], [5], therefore β_1 equals to β_2. Then, the transfer function of a TLC can be derived as follows.

$$S_{21} = \frac{b_2(0)}{a_1(0)} = \frac{jK\sin(\omega L/v_p)}{\sqrt{1-K^2}\cos(\omega L/v_p) + j\sin(\omega L/v_p)}, \tag{6}$$

$$S_{31} = \frac{a_1(L)}{a_1(0)} = \frac{\sqrt{1-K^2}}{\sqrt{1-K^2}\cos(\omega L/v_p) + j\sin(\omega L/v_p)}. \tag{7}$$

where v_p is phase velocity and the definition of ports is shown in Fig. 6.

As Eq. (6) shows, transfer from Port 1 to Port 2, S_{21}, is maximized to K when $f_c = v_p/4L$. The transfer function of a TLC depends on coupling the coefficient, K, and the length of the coupler, L. Figure 7 shows simulation results when L = 3mm, d = 0.08mm, W = 0.3mm, h = 0.4mm. A TLC has a bandpass transfer function as Eq. (6) and Fig. 7 show. S_{11} in Fig. 7 is well below −10dB. By choosing W, h, d, and S appropriately, a signal can be transferred through a TLC while minimizing reflections. Note that Eqs. (6) and (7) stand only when ports are terminated with impedance matching and a TLC consists of a uniform dielectric material. Otherwise the electric coupling and magnetic coupling are not balanced and the coupling coefficient K is an addition of electric and magnetic coupling [5].

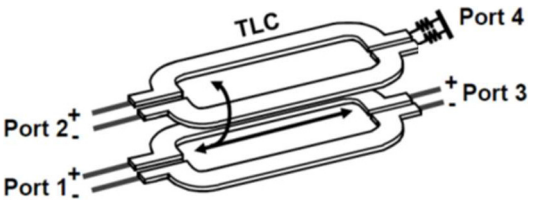

Fig. 6 Definition of ports in TLC.

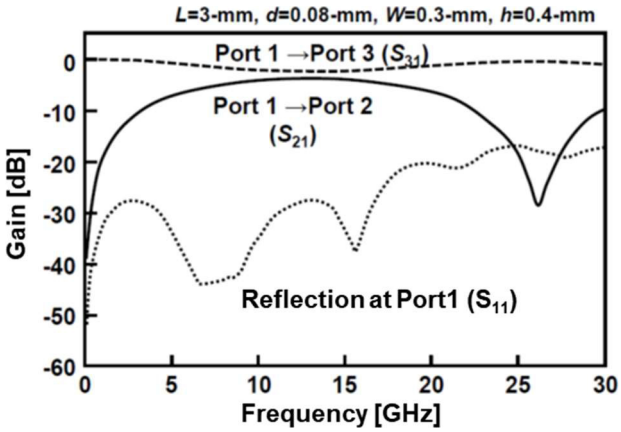

Fig. 7 Frequency response of gain of TLC.

2.3 Design Methodology

A relation between the coupling coefficient K and design parameters of a TLC can be obtained from Eq. (6). The coupling coefficient K is expressed by even mode capacitance C_{even} and odd mode capacitance C_{odd} as [6],

$$K = (C_{odd} - C_{even})/(C_{odd} + C_{even}). \tag{8}$$

As Fig. 8 shows, in an even mode, electric potential of the primary and the secondary is balanced, and capacitance in between is zero, therefore $C_{even} = C_{11} = C_{12}$. On the other hand, in an odd mode, electric potential of the primary and the secondary is differential, capacitance in between is $2C_{21}$ due to Miller effect, therefore $C_{odd} = C_{11} + 2C_{21} = C_{22} + 2C_{21}$. The coupling capacitance C_{21} depends on a ratio of W to d, and self-capacitance, C_{11} and C_{22}, depends on a ration W to h. When capacitance in Eq. (8) is approximated

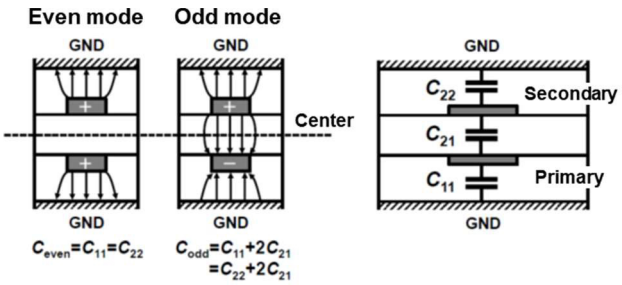

(a) E-field and effective capacitance (b) Self and coupling capacitance

Fig. 8 Electric field and capacitance in even/odd mode.

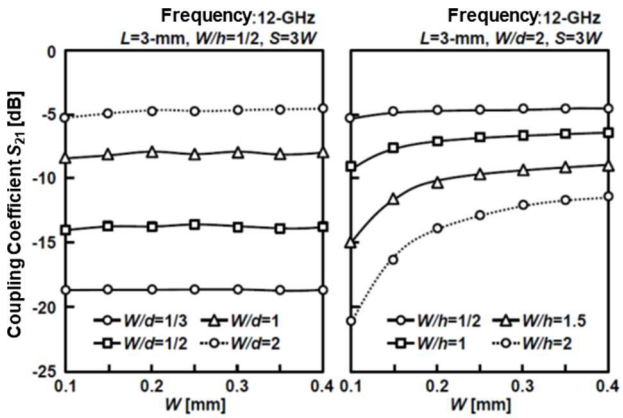

(a) W/h fixed at1/2 (b) W/d fixed at 2

Fig. 9 Simulation results of coupling coefficient of TLC.

simply by the parallel plate model, the coupling coefficient K is expressed by d, h, and W as follows.

$$K = \frac{\varepsilon_0\varepsilon_r\frac{W}{d} + C_{m,fr}}{\varepsilon_0\varepsilon_r\frac{W}{d} + C_{m,fr} + 2C_{s,fr} + \varepsilon_0\varepsilon_r\frac{W}{h}} \tag{9}$$

where $C_{m,fr}$ and $C_{s,fr}$ are fringe capacitance in the coupling capacitance and self-capacitance respectively, and ε_0 is dielectric constant in vacuum.

Equation (9) tells us that the coupling coefficient can be tuned by two ratios, W to h and W to d. Figure 9 shows results of 3-D electromagnetic simulations with varying W/d and W/h.

It is clear that the transfer from the primary to the secondary is a strong function of W/d or W/h and a weak function of the absolute value of W when $W > 0.2$ mm.

In order to increase the transfer from the primary to the secondary, the spacing between differential transmission lines, S, is required to be increased to weaken their coupling. To see the effect, in Fig. 10 (a), simulation results of S_{21} is shown with varying S/W. It shows that S_{21} is saturated above S/W of 3. When two couplers are placed side by side, crosstalk is reduced less than −20dB to the signal when the spacing between two couplers is >2.3W as shown in Fig. 10 (b). Therefore an effective pitch of the coupler should be $W + S + W + Z > 7.3W$ to obtain a sufficient signal-to-noise ratio. As described in Sect. 2.2, the center

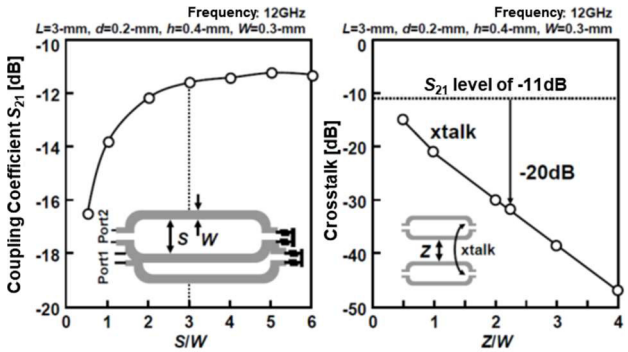

(a) S_{21} vs. S/W (b) Xtalk vs Z/d

Fig. 10 Simulation results of S_{21} and crosstalk of TLC.

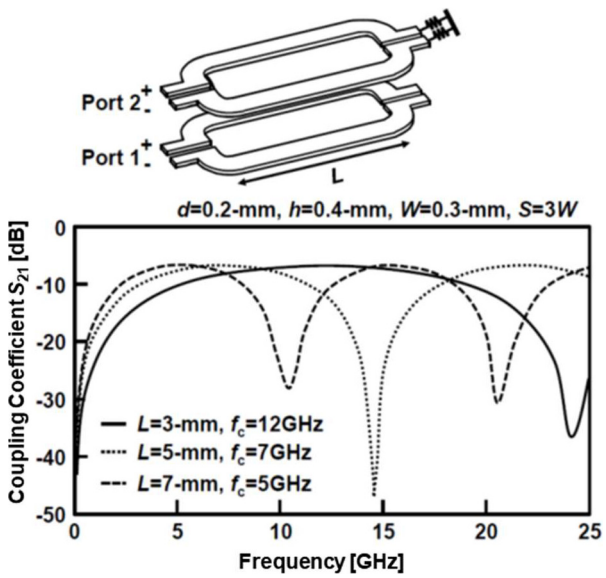

Fig. 11 Simulation results of S_{21} with different L of TLC.

frequency of the transfer function of a TLC is $v_p/4L$, which, in turn, the shorter L, the higher the center frequency and the wider the 3-dB bandwidth as Fig. 11 shows. Here, we look into the relation between L and rise/fall time of the secondary signal. The secondary signal is derived from Eq. (1) as,

$$V_{RX}(t) = \frac{K}{v_p}\int_{z=0}^{L}\frac{dV_{TX}(t-2z/v_p)}{dt}dz. \tag{10}$$

By plugging the primary signal as a sigmoid function (a step function) into Eq. (10),

$$V_{RX}(t) = \frac{K}{2}\left\{V_{TX}(t) - V_{TX}\left(t-\frac{2L}{v_p}\right)\right\}. \tag{11}$$

The equation shows that the secondary signal is a pulse function, whose maximum amplitude V_{RX_P}, and pulse width t, depend on L and rise time of the primary signal, T_r, which is expressed as follows.

$$V_{RX\_P} = \frac{K}{2}V_{TX\_P} \qquad (T_r v_p/2 < L)$$

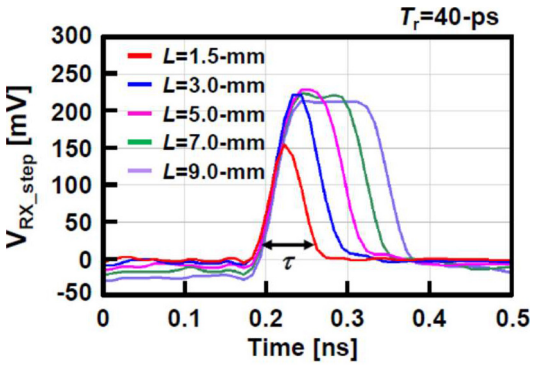

(a) with different L

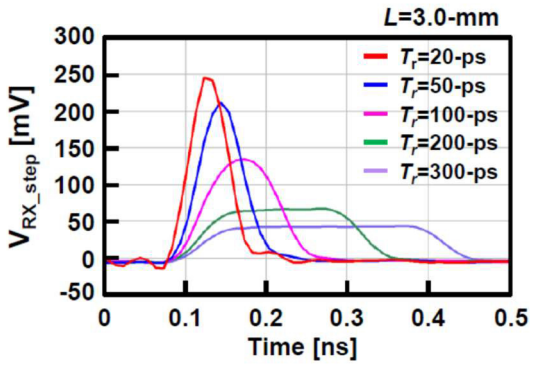

(b) with different T_r

Fig. 12 Simulation results of step response of TLC.

$$V_{RX\_P} = \frac{KL}{v_p T_r} V_{TX\_P} \qquad (T_r v_p/2 > L). \tag{12}$$

$$\tau = T_r + \frac{2L}{v_p}. \tag{13}$$

These analytical expressions are confirmed by simulation. The results are shown in Fig. 12. As L becomes longer, the secondary signal amplitude becomes larger until it saturates when

$$L \le T_r v_p/2. \tag{14}$$

The length of a TLC should be $T_r v_p/2$ to obtain the maximum secondary amplitude and the minimum inter-symbol interference.

3. Applications of TLC

3.1 Two-Fold Transmission Line Coupler (T-TLC) [7]

Modular smart phones as shown in Fig. 13 have been attracting attention because users can freely customize their phones by purchasing modules and assembling them. The transfer of data between modules is accomplished by non-contact connectors. For this application, one of the shortcomings of the TLC is that the space occupied by the coupler increases as the connection distance increases. The

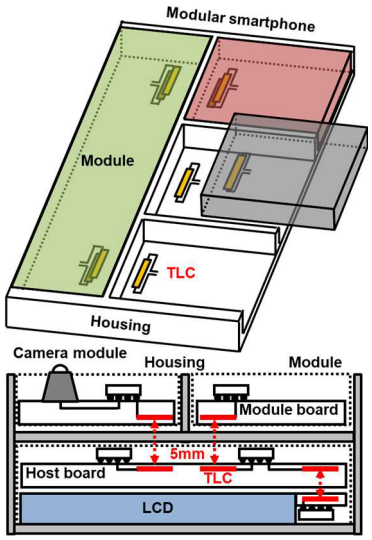

Fig. 13 Non-contact interface for modular smartphone.

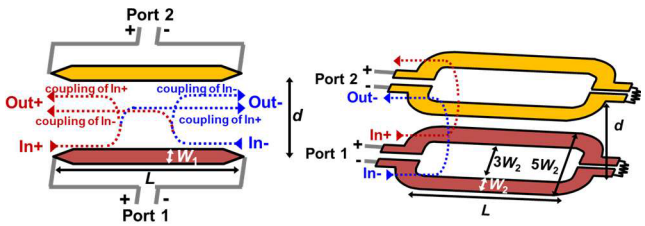

(a) T-TLC (b) conventional TLC

Fig. 14 Two-fold transmission line coupler (T-TLC).

coupling gain of the TLC is determined by the ratio of the electrode width (W) and the connection distance (d). The bandwidth (BW) is determined by the electrode length (L). In a typical design, the electrode width (W) is 0.5 mm for the parameter values of d = 1 mm, L = 5 mm, and BW = 6.4 GHz. If the maximum connection distance for a modular smart phone is 5 mm, the maximum electrode width (W) is 2.5 mm, which is too large. Small TLC's that can be used for small modules are also needed.

Figure 14 shows a two-fold transmission line coupler (T-TLC) that is compact and can connect at 5 mm. The T-TLC is capable of differential coupling with half the number of electrodes as the conventional TLC and the width can be reduced from $5W_2$ to W_1, where W_1 and W_2 is the electrode width of the T-TLC and the conventional TLC, respectively. With a conventional TLC, communication can use only backward positive coupling, because the signal from forward negative coupling is lost due to the termination resistance. With the T-TLC, however, the backward positive coupling signal of the forward input (In+) and the forward negative coupling signal of the backward input (In-) are added to produce the forward output (Out+). As a result, the coupling gain is increased by 6 dB. Besides the coupling gain of a conventional TLC is reduced by 3 dB due to cross coupling between differential signals running in

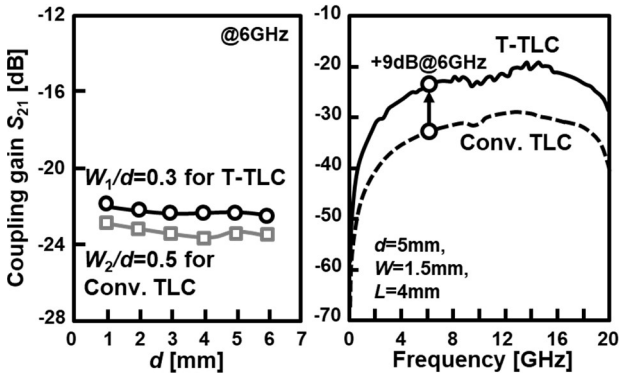

Fig. 15 Coupling coefficient vs. frequency and distance.

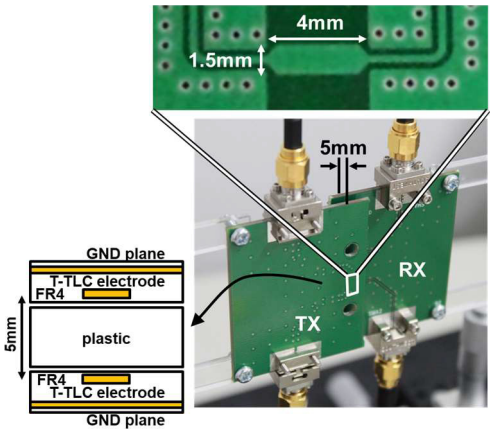

Fig. 16 Photographs of fabricated T-TLC.

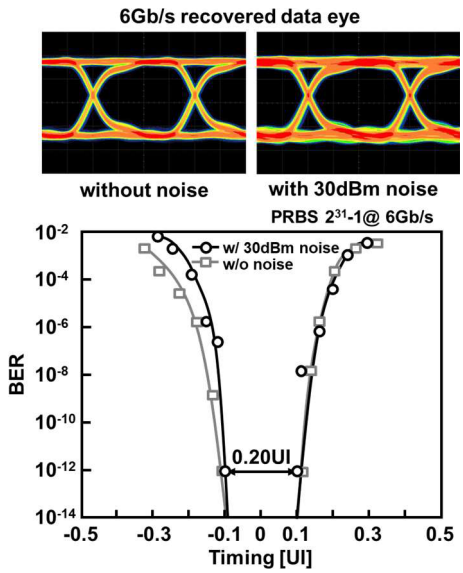

Fig. 17 Bathtub curves with/without noise injection.

parallel when the electrode width is $3W_2$, but there is no such parallel propagation of differential signals with the T-TLC, so there is no such reduction of coupling gain. Because of the total coupling gain increase of 9 dB, the electrode width of the T-TLC can be reduced from the $W_2/d = 0.5$ of the conventional TLC to $W_1/d = 0.3$, which has an even larger gain as shown in Fig. 15. By combining the effects of reducing the number of electrodes and increasing the coupling gain, it is possible to reduce the overall width of the coupler from $5W_2 = 12.5$ mm to $W_1 = 1.5$ mm (a factor of 1/8.3). Additionally, the T-TLC can be terminated within the transceiver chip, so no external resistance is needed and the surface area can be reduced even further. As there is no such reduction of coupling gain due to parallel propagation of differential signals, the T-TLC has larger tolerance against horizontal offset (δ) than the conventional TLC. A 1-dB compression point of the coupling gain is increased from $\delta = 0.4\ W_2$ (= 1 mm) in the conventional TLC to $0.8\ W_1$ (= 1.2 mm) in the T-TLC, resulting in negligibly small restriction in alignment error.

For parameter values of $d = 5$ mm, $W = 1.5$ mm, and $L = 4$ mm, the bandwidth of the T-TLC is 16 GHz. It will be possible to transfer 4K video data (15 Gb/s) over a single lane.

For demonstration of the technology, the T-TLCs were fabricated on a four-layer FR4 substrate that is 1.6 mm thick. The T-TLC electrodes were formed on layer 1 and a ground plane for shielding was formed on layer 4, with a separation of 1.5 mm. Their photographs are shown in Fig. 16. Communication experiments were performed at the MIPI maximum data transfer rate of 6 Gb/s at a communication distance of 5 mm, where bathtub curves are measured to show noise immunity. A 30 dBm Wi-Fi signal (2.4 GHz) served as a noise source positioned slightly to the outside of the minimum separation, for which the BER is 10^{-12}. Holding the receiver clock phase constant, the BER was measured as the transmission data phase was varied. As shown in Fig. 17, even with the noise, the timing margin for maintaining the BER at less than 10^{-12} was decreased by only 0.02 UI and a wide timing margin of 0.20 UI was obtained.

3.2 Single-Ended to Differential Conversion Transmission Line Coupler (SDC-TLC) [8]

In order to reduce the width of the memory modules we developed the single-ended to differential conversion TLC (SDC-TLC) as a high mounting density coupler. It can convert a single-end signal to a differential signal and can be used in a multidrop bus configuration. Five memory devices and a memory controller in FPGA can be connected by a bus as shown in Fig. 18, so the number of signal wires can be reduced by 80% and the width of the memory module can be reduced. In a multidrop bus configuration, the incoming DDR4 single-end signal at each branch is converted to a differential signal by the SDC-TLC, and restored to a digital signal by a differential receiver.

We explain the SDC-TLC operating principle for the conversion from a single-end signal to a differential signal by using Fig. 19. The single-end signal input from port

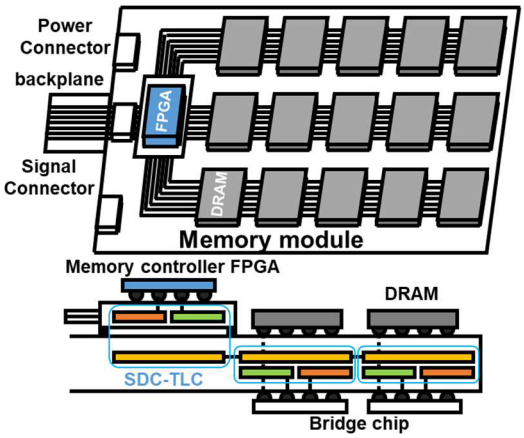

Fig. 18 Memory module employing SDC-TLCs.

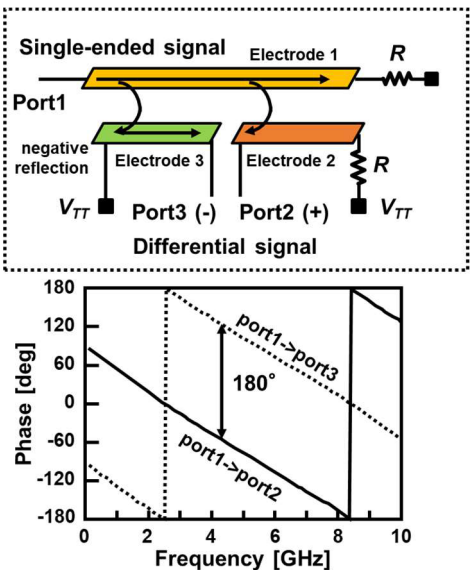

Fig. 19 SDC-TLC with its frequency response.

1 to electrode 1 generates a signal in electrode 3 that has the same symbol but opposite direction. That signal is completely reflected at the shorted end of the electrode, which reverses the phase by 180°, and the signal proceeds to port 3 as an inversion of the input signal. When the input signal proceeds past the midpoint of electrode 1, it generates a signal in electrode 2 that has the same symbol but opposite direction. That signal has the same phase as the input signal and proceeds to port 2. Accordingly, the single-end signal that was input at port 1 appears as a differential signal at ports 2 and 3. Similarly, in the reverse direction, a differential signal input from port 2 and port 3 arrives at port 1 as a single-end signal. Because two couplers are arranged in series, the layout area in the length direction is twice as long. However, only one fourth the area is needed in the width direction, so the SDC-TLC occupies only 4.2 mm^2, a reduction by 55% compared to the conventional TLC. The SDC-TLCs were formed in the metal traces on a printed circuit board of FR4 as shown in Fig. 20. Tests for the memory module were performed at 3.2 Gb/s to match the DDR4 memory interface. The bit error rate with six modules connected was confirmed to be less than 10^{-12} with timing margin of 0.67 UI.

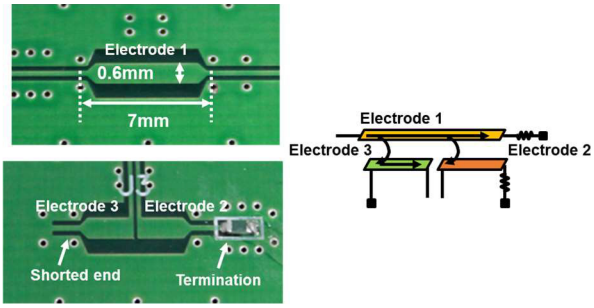

Fig. 20 Fabricated SDC-TLCs.

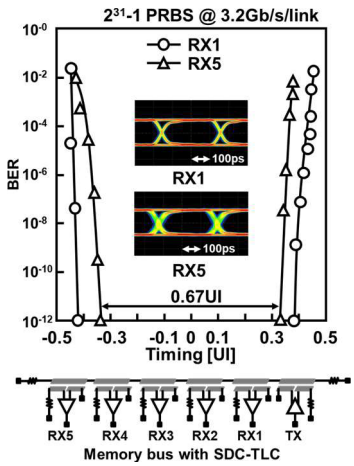

Fig. 21 Measured bathtub curves and eye diagrams of SDC-TLC.

3.3 Rotatable Transmission Line Coupler (RTLC) [9]

Conventional TLCs are sensitive to angular rotation whose coupling gain varies and falls below a required level. Therefore, they are not applicable for rotatable connecters, such as ones in robot arms.

The rotatable transmission line coupler (RTLC) is developed which has a constant coupling gain at all rotation angles as shown in Fig. 22. A conventional TLC is rectangular and its coupling gain varies depending on the size of overlapped area in the rotation. The proposed doughnut-shaped RTLC has a constant overlapped area at any rotation angle. Therefore, the coupling gain is also constant. The bandwidth of TLC depends on the coupling line length. The coupling line length of RTLC varies with the rotation angle θ. At θ = 180deg, the bandwidth becomes the narrowest thus inter-symbol interference becomes critical, which can be managed in the receiver circuit. As for the dimension design, smaller diameter D decreases the coupling length and results in a wider bandwidth. A larger coupler width W increases its coupling gain, however, increases the coupler length so that its bandwidth decreases. In this work, D and

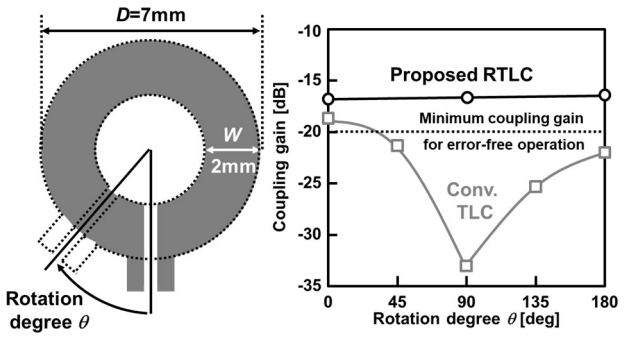

Fig. 22 Rotatable transmission line coupler (RTLC).

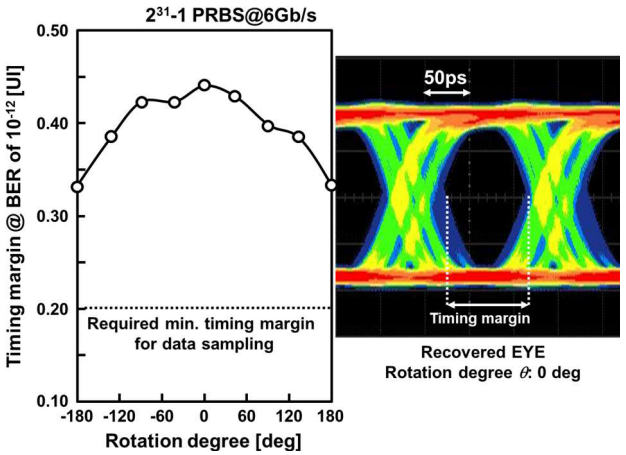

Fig. 23 Measured timing margin of RTLC.

W are set to 7mm and 2mm, respectively.

The 6Gb/s PRBS $2^{31} - 1$ signal was transmitted via RTLC. As shown in Fig. 23, measured BER was lower than 10^{-12} at any rotation angle in a communication distance of 3mm.

4. Conclusions

In this paper, the transmission line coupler was reviewed. The characteristics of a TLC was analyzed and its design methodology was presented. In order to show its versatility for a compact and high-speed non-contact connecter, we reviewed three different types of applications, T-TLC, SDC-TLC, and RTLC.

Acknowledgments

This work was supported by JST ACCEL Grant Number JPMJAC1502, Japan. The authors thank Drs. Take and Kosuge for their invaluable support.

References

[1] D. Mizoguchi, Y.B. Yusof, N. Miura, T. Sakurai, and T. Kuroda, "A 1.2Gb/s/pin Wireless Superconnect based on Inductive Inter-chip Signaling (IIS)," IEEE International Solid-State Circuits Conference (ISSCC'04), Dig. Tech. Papers, pp.142–143, Feb. 2004.

[2] T. Takeya, L. Nan, S. Nakano, N. Miura, H. Ishikuro, and T. Kuroda, "A 12Gb/s Non-Contact Interface with Coupled Transmission lines," IEEE International Solid-State Circuits Conference (ISSCC'11), Dig. Tech. Papers, pp.492–493, Feb. 2011.

[3] http://pcisig.com/

[4] N. Kinayman and M.I. Aksun, Modern Microwave Circuits, Artech House, London, UK, 2005.

[5] M.K. Krage and G.I. Haddad, "Characteristics of Coupled Microstrip Transmission Lines-I: Coupler-Mode Formulation of Inhomogeneous Lines," IEEE Trans. Microw. Theory Techn., vol.18, no.4, pp.217–222, April 1970.

[6] D.M. Pozar, Microwave Engineering, 4th ed., Wiley, Hobboken, NJ, USA, 2011.

[7] A. Kosuge, S. Ishizuka, J. Kadomoto, and T. Kuroda, "A 6Gb/s 6pJ/b 5mm-Distance Non-Contact Interface for Modular Smartphones Using Two-Fold Transmission Line Coupler and EMC-Qualified Pulse Transceiver," IEEE International Solid-State Circuits Conference (ISSCC'15), Dig. Tech. Papers, pp.176–177, Feb. 2015.

[8] A. Kosuge, S. Ishizuka, M. Abe, S. Ichikawa, and T. Kuroda, "A 6.5Gb/s Shared Bus using Electromagnetic Connectors for Downsizing and Lightening Satellite Processor System by 60%," IEEE International Solid-State Circuits Conference (ISSCC'15), Dig. Tech. Papers, pp.434–435, Feb. 2015.

[9] M. Haraguchi, A. Kosuge, T. Igarashi, S. Masaki, M. Sueda, M. Hamada, and T. Kuroda, "A 6Gb/s Rotatable Non-Contact Connector with High-Speed/I2C/CAN/SPI Interface Bridge IC," IEEE Symposium on VLSI Circuits, Dig. Tech. Papers, pp.C150–C151, June 2017.

Mototsugu Hamada received the B.S., M.S., and Ph.D. degrees in electronic engineering from the University of Tokyo, Tokyo, Japan, in 1991, 1993, and 1996, respectively. In 1996, he joined Toshiba Corporation and has been engaged in wireless and lowpower electronic circuits design with Center for Semiconductor Research and Development, Kawasaki, Japan. In 2016, he joined Keio University and is currently a Research Professor.

Tadahiro Kuroda received the Ph.D. degree in electrical engineering from the University of Tokyo, Tokyo, Japan, in 1999. In 1982, he joined Toshiba Corporation, where he engaged in the research and development of BiCMOS/ECL ASICs, high-speed CMOS LSIs for telecommunications and low-power CMOS LSIs for mobile applications. In 2000, he moved to Keio University, Yokohama, Japan, where he has been a professor since 2002. He is an IEEE Fellow and an IEICE Fellow.